

Learned Display Radiance Fields with Lensless Cameras

Ziyang Chen
University College London
London, United Kingdom
ziyang.chen.22@ucl.ac.uk

Yuta Itoh
University of Tokyo
Tokyo, Japan
yuta.itoh@iii.u-tokyo.ac.jp

Kaan Akşit
University College London
London, United Kingdom
k.aksit@ucl.ac.uk

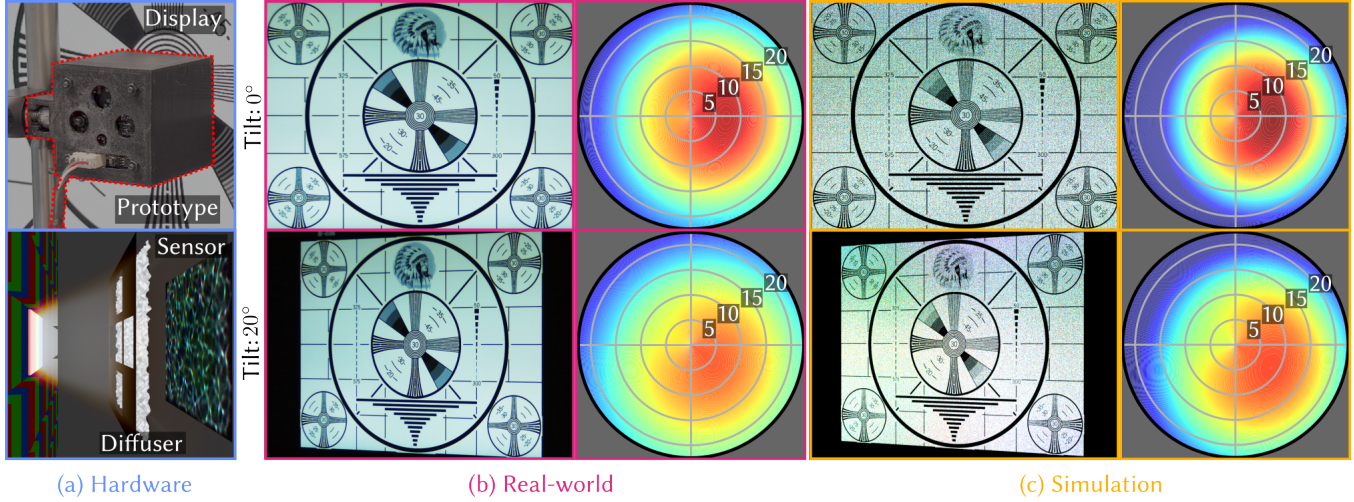


Figure 1: (a) Our lensless camera placed in front of the display captures the light field emitted from the display pixels. (b) A conventional camera captures a real-world photograph of the test pattern on the display. (c) Our learned model estimates a rendered view from the viewpoint of the real-world photograph displayed in the middle column. The right columns in (b) and (c) present the display’s angular intensity distributions in spherical coordinates. The radius denotes the combined angular deviation from the optical axis, computed from the horizontal and vertical incidence angles. These plots illustrate how the relative intensity changes with viewing angle.

Abstract

Calibrating displays is a basic and regular task that content creators must perform to maintain optimal visual experience, yet it remains a troublesome issue. Measuring display characteristics from different viewpoints often requires specialized equipment and a dark room, making it inaccessible to most users. To avoid specialized hardware requirements in display calibrations, our work co-designs a lensless camera and an Implicit Neural Representation based algorithm for capturing display characteristics from various viewpoints. More specifically, our pipeline enables efficient reconstruction of light fields emitted from a display from a viewing cone of $46.6^\circ \times 37.6^\circ$. Our emerging pipeline paves the initial steps towards effortless display calibration and characterization.

CCS Concepts

• **Hardware** → Emerging simulation; Hardware validation; • **Computing methodologies** → Computational photography.

Keywords

Lensless camera, Implicit Representation, Display calibration

1 Introduction

Professional content creators use off-the-shelf colorimeters¹ regularly to maintain a color consistency in the workflow. Similarly, display engineers conduct calibrations by measuring various aspects of screens including but not limited to luminance, chromaticity, and contrast ratios². This process requires specialized equipment such as spectroradiometers or goniophotometers³.

Display chromaticity and luminance vary with viewing angle, affecting how users perceive content from different positions in front of a screen. But most calibration tools assume a fixed viewing position leading to invalid assessments for other viewing positions. This is not only problematic for display manufacturers but also for professionals that need consistent color edits for various geometric configurations. The ISO standards [2] define procedures for assessing the uniformity distribution of Flat Panel Displays (FPD) at various viewing directions by rotating either the display or measurement instrument in a dark room. However, these requirements with numerous captures hinder the end users from performing

¹<https://www.adobe.com/creativecloud/video/discover/how-to-calibrate-monitor.html>

²<https://www.admesy.kr/articles/display-calibration-workflows-rd-to-mass-production/>

³<https://www.lisungroup.com/news/technology-news/application-of-goniophotometers-in-display-and-projection-technologies.html>

regular calibration, which is critical for applications such as virtual production display walls⁴, professional workstations in graphic design, video editing⁵, and automotive dashboard systems [3]. *An accessible method with a reasonable amount of captures is needed to measure the image quality of the displays from arbitrary viewpoints.*

Our work introduces a calibration tool that characterizes the display pixel emission patterns at different viewing angles with simpler setup and fewer captures. Specifically, we design a paired hardware and software: (1) a lensless camera [1, 4] capturing the incoming light of a display pixel from a range of directions and (2) an Implicit Neural Representation (INR) that encodes the display angular responses. Our work makes the following contributions:

- **Lensless Camera Prototype.** We design a lensless camera using a phase mask and aperture array to capture display characteristics across a practical angular range. The phase mask is positioned 30 mm from the display pixel, with the imaging sensor placed 10 mm behind it to ensure spatial invariance of the diffuser. This configuration enables horizontal and vertical incident angle coverage of approximately 46.6 and 37.6 degrees, respectively.
- **INR for Display Pixel Characterization.** To efficiently represent the light fields from the lensless captures and generate novel views of unseen display pixels, we train a Multi-Layer Perceptron (MLP) that performs end-to-end reconstruction based on different display positions and incident angles. This MLP model can be trained with only **nine** positions on the display, enabling the reconstruction of the light field for each pixel on the display.

We conduct experiments on a Liquid Crystal display (LCD) display and demonstrate that our method can reconstruct the display with different viewpoints. Our codebase and hardware design will be available upon acceptance.

2 Methods

Our method reconstructs the light field representation of a display from lensless captures of individual pixels. We detail our pipeline consisting hardware and software components in the subsequent sections. The notations used throughout this section are summarized in Tbl. 1. Upper-case bold letters denote matrices, while lower-case bold letters represent vectors. Scalars and spatial indices are denoted by non-boldface letters. The calligraphic letters indicate the functions. These notations will be consistently used to formalize the forward model and reconstruction process in the following subsections.

2.1 Lensless 2D Image Formation

Capturing the incoming light from pixels across multiple directions is crucial in our application. We choose the lensless cameras for their ease of modification and flexibility.

\mathbf{H}	Coefficient matrix for lensless forward model
\mathbf{Y}	Lensless camera 2D measurements
\mathbf{X}	Lensless camera unknown scene intensity
\mathbf{y}	Flattened lensless camera measurements
\mathbf{x}	Flattened unknown scene intensity
h_I, w_I	Height and width of the lensless image
h_S, w_S	Height and width of the scene
$\mathcal{C}(\cdot)$	Cropping function
$\mathcal{Z}(\cdot)$	Zero padding function
\mathbf{h}	Pre-captured PSF
x, y	Display pixel coordinates
u, v	Light field angular coordinates
s, t	Image coordinates
\mathbf{L}	Light field
\mathbf{I}_{pred}	Predicted lensless capture
\mathbf{I}_{gt}	Ground truth lensless capture
\mathcal{F}_θ	Multi-layer perceptron
$\gamma(\cdot)$	Positional encoding
n	Aperture size
m	Distance between display pixel and aperture
α	Incident angle of the light rays

Table 1: Notation used throughout this section.

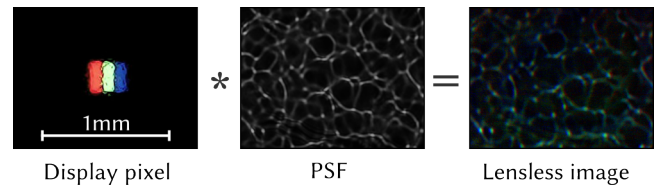


Figure 2: The display pixel captured with a microscope (left). The Point Spread Function (PSF) captured with the proposed lensless camera (middle). The captured lensless image from the display pixel (right).

Our lensless camera contains a diffuser that alters the light propagation paths, resulting in distorted images on the sensor as shown in Fig. 2. Let h_I and w_I denote the height and width of the sensor, and h_S and w_S denote the height and width of the scene. The forward imaging process can be expressed as

$$\mathbf{y}_I = \mathbf{H}\mathbf{x}_S, \quad (1)$$

where $\mathbf{y}_I \in \mathbb{R}^{(h_I \cdot w_I) \times 1}$ denotes the flattened measurement vector from the sensor, $\mathbf{H} \in \mathbb{R}^{(h_I \cdot w_I) \times (h_S \cdot w_S)}$ is a coefficient matrix modeling the input light's interaction with the diffuser, and $\mathbf{x}_S \in \mathbb{R}^{(h_S \cdot w_S) \times 1}$ represents the flattened intensity vector of the unknown scene. However, reconstructing the full \mathbf{H} matrix is computationally intractable. To address this, we position the diffuser close to the sensor to ensure spatial invariance in the forward model, allowing it to be approximated as a linear convolution:

$$\begin{aligned} \mathbf{Y} &= \mathcal{C}(\mathcal{Z}(\mathbf{X}) * \mathcal{Z}(\mathbf{h})) \\ &= \mathcal{F}^{-1}(\mathcal{F}(\mathcal{C}(\mathcal{Z}(\mathbf{X}))) \cdot \mathcal{F}(\mathcal{Z}(\mathbf{h})),) \end{aligned} \quad (2)$$

where $\mathbf{Y} \in \mathbb{R}^{h_I \times w_I}$ denotes the 2D measurements, $\mathbf{X} \in \mathbb{R}^{h_S \times w_S}$ denotes the unknown scene intensity, $*$ denotes the 2D linear convolution operation, $\mathcal{C}(\cdot)$ is the cropping operation, \cdot is the Hadamard

⁴<https://partnerhelp.netflixstudios.com/hc/en-us/articles/1500002086641-Common-Virtual-Production-Challenges-Potential-Solutions>

⁵<https://displaycal.net/>

product, $\mathcal{Z}(\cdot)$ is the zero padding operation to ensure dimension consistency and avoids circular convolution artefact, \mathcal{F} and \mathcal{F}^{-1} denote the Discrete Fourier Transform (DFT) and Inverse DFT (IDFT), respectively, and $\mathbf{h} \in \mathbb{R}^{h_s \times w_s}$ is the pre-captured PSF. To reconstruct for the unknown scene \mathbf{X} , we need to solve an inverse problem of the Eq. (2) by minimizing the loss:

$$\hat{\mathbf{X}} \leftarrow \underset{\mathbf{X}}{\operatorname{argmin}} \mathcal{L}(\mathbf{Y}_{\text{gt}}, C(\mathcal{Z}(\mathbf{X}) * \mathcal{Z}(\mathbf{h}))), \quad (3)$$

where \mathbf{Y}_{gt} is the ground truth lensless image.

2.2 Lensless Light Field Formation

We leverage the lensless camera system to capture the unknown light fields for pixels at different locations on the display $\mathbf{L} = (u, v, s, t)$, where the (u, v) and (s, t) are the angular and spatial coordinates. An image formed by the directional light rays from a single or multiple light sources satisfies:

$$\mathbf{I}(s, t) = \int_{\Omega_x} \int_{\Omega_y} \mathbf{L}(u, v, s, t) du dv, \quad (4)$$

where $\{\Omega_x, \Omega_y\}$ is a subset of all the angles which the light rays reach for the imaging sensor. To simplify the problem, we model the phase mask as an array of pinholes that scatter incident light rays arriving at angles (u', v') onto the imaging sensor, forming distinct patterns that we refer as sub-aperture images. The formation of each sub-aperture image can be modeled as the 2D convolution of the scene information with its corresponding PSF patch, $\mathbf{h}(u', v')$. To compute this convolution efficiently across all angular dimensions, we employ a 4D DFT on the spatial coordinates:

$$\mathbf{I}_{\text{gt}} = \mathcal{F}^{-1} \left(\mathcal{F} \left(C(\mathcal{Z}(\mathbf{L})) \right) \cdot \mathcal{F} \left(\mathcal{Z}(\mathbf{h}) \right) \right). \quad (5)$$

Finally, we pose the recovery of the light field as an inverse problem:

$$\hat{\mathbf{L}} \leftarrow \underset{\mathbf{L}}{\operatorname{argmin}} \mathcal{L}(\mathbf{I}_{\text{gt}}, C(\mathcal{Z}(\mathbf{L}) * \mathcal{Z}(\mathbf{h}))), \quad (6)$$

where \mathbf{I}_{gt} denotes the ground truth lensless capture.

2.3 Implicit Neural Representation

We utilize an MLP to efficiently represent the continuous pixel light field samples from the lensless captures to avoid extensive sampling on the target screen, which satisfies:

$$\hat{\mathbf{L}}(\mathbf{x}, \mathbf{y}, u, v, s, t) = \mathbf{F}_\theta(\mathbf{x}, \mathbf{y}, u, v, s, t), \quad (7)$$

where \mathbf{F}_θ is an MLP with parameters θ . This network takes the spatial and angular coordinates as input and outputs the corresponding pixel color value. The variables \mathbf{x} and \mathbf{y} denote the illuminated pixel coordinates on the display. Before the input coordinates are fed into the MLP, we apply positional encoding [5] to the coordinates to increase the model’s capacity to learn high-frequency details:

$$\gamma(p) = \left(\sin(2^0 \pi p), \cos(2^0 \pi p), \dots, \sin(2^{L-1} \pi p), \cos(2^{L-1} \pi p) \right), \quad (8)$$

We apply the positional encoding with different frequency levels in the input coordinate groups: $\mathbf{e} = (\gamma_0(\mathbf{x}, \mathbf{y}), \gamma_1(u, v), \gamma_1(s, t))$. Finally, the minimization problem in Eq. (6) is reformulated as:

$$\hat{\theta} \leftarrow \underset{\theta}{\operatorname{argmin}} \mathcal{L}(\mathbf{I}_{\text{gt}}, C(\mathcal{Z}(\mathbf{F}_\theta(\mathbf{e})) * \mathcal{Z}(\mathbf{h}))), \quad (9)$$

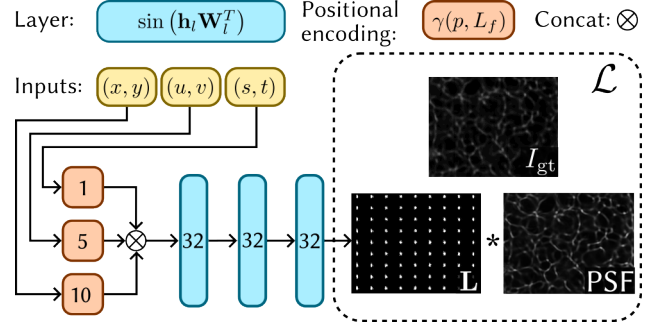


Figure 3: Each MLP layer consists of 32 neurons and a sinusoidal activation function. We apply positional encoding with varying frequency levels (L_f) to each input coordinate group. After concatenating these encoded features, the model processes them to reconstruct the light field. We then perform linear convolution between this reconstruction and the pre-captured PSF to generate the predicted lensless image (\mathbf{I}_{pred}). Finally, we compute the loss with \mathbf{I}_{pred} and \mathbf{I}_{gt} .

where $\hat{\theta}$ denotes the optimized parameters of the MLP.

Loss function. We employ the L_1 norm to quantify the discrepancy between \mathbf{I}_{pred} and \mathbf{I}_{gt} , and use \mathcal{R} to penalize predicted pixel values exceeding the range $[0, 1]$. We define:

$$\mathcal{R}(\mathbf{I}_{\text{pred}}) = \sum \max(\mathbf{I}_{\text{pred}} - 1, 0) + \sum \max(-\mathbf{I}_{\text{pred}}, 0). \quad (10)$$

The total training loss is then:

$$\mathcal{L} = \lambda_0 \|\mathbf{I}_{\text{gt}} - \mathbf{I}_{\text{pred}}\|_1 + \lambda_1 \mathcal{R}(\mathbf{I}_{\text{pred}}), \quad (11)$$

where λ_0 , and λ_1 represent weights ($\lambda_0 = 1$, $\lambda_1 = 10^{-7}$).

3 Evaluation and Discussion

Hardware. Our hardware setup consists of a 0.5° engineered diffuser (Edmund 35-860) with an array of five $2.5 \text{ mm} \times 3 \text{ mm}$ apertures serving as a mask positioned 10 mm from the imaging sensor as illustrated in Fig. 4. This distance is experimentally determined to ensure spatial invariance of the diffuser and the sharpest caustic pattern, satisfying condition in Eq. (2). We 3D print a housing that maintains a fixed 30 mm distance between the diffuser and screen pixel, as the left image in Fig. 5 demonstrates. We capture a stack of PSF for each aperture by positioning the lensless camera in front of a white LED coupled to a $100 \mu\text{m}$ pinhole (Thorlabs P100HKb). We mount the prototype in front of the display panel and turn on each pixel one by one to capture the light fields. We choose the position of activated pixel relative to the corresponding aperture to ensure the light rays pass through the aperture and reach the imaging sensor. We detail this process in Supplementary Sec. 1.

Implicit Neural Representation. We divide the lensless captures into 9×9 sub-aperture images using a sliding window of size 54×70 pixels. Later we feed them into our MLP that consists of 3 fully connected layers with sinusoidal activation functions, each containing 32 channels. Before inputting the coordinates described in Sec. 2.3, we inject random noise into each coordinate group, which helps improve generalization: display coordinates (std: $5 \times$

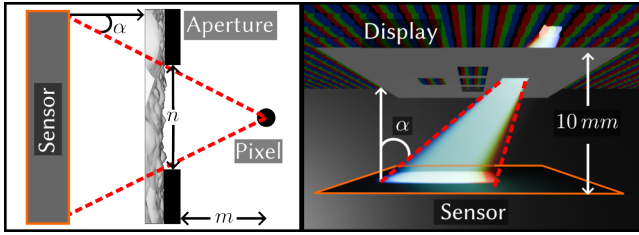


Figure 4: The incident angle (α) of the light rays is determined by the distance between the aperture and the display pixel (m), as well as the size of the aperture (n) (left). Our proposed aperture array expands the incident angle range by turning on each pixel one by one (right).

10^{-3}), angular coordinates (std: 1×10^{-2}), and subview coordinates (std: 1×10^{-3}). Subsequently, we apply the positional encoding function Eq. (2.3) with one frequency level for display coordinates, five for angular coordinates, and ten for spatial coordinates, as illustrated in Fig. 3. We analyze the choices of frequency levels in Supplementary Sec. 2 to ensure the model is generalized to unseen pixel position and viewpoints. We optimize our model using the Adam optimizer with an initial learning rate of 0.001 that decays linearly over 800 epochs. To prevent gradient explosion during early training, gradient norms are clipped to 1.0. We train the model on independent color channels to mitigate crosstalk, which takes about one hour on a single NVIDIA RTX 2070 GPU, while inference requires roughly 0.01 seconds per 1080p frame.

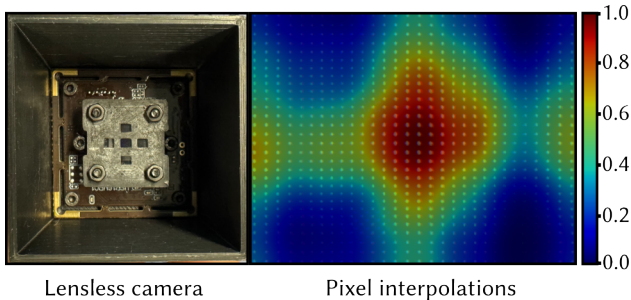


Figure 5: The top view of our lensless camera (left). The simulated display pixels with unseen incident angles and the corresponding overlay intensity heatmap (right).

Quantitative Evaluations. We assess pixel consistency by measuring how well the reconstructed light fields preserve intensity variations across continuous horizontal and vertical incident angles. Fig. 5 shows that the average pixel intensity changes smoothly, indicating that our model can predict novel, angle-dependent pixel values. We compare our architecture against a vanilla MLP baseline consisting of fully connected layers with ReLU activations in Tbl. 2. Our method achieves higher scores in all metrics, demonstrating superior performance. To benchmark our method, we follow the ISO [2] standard: a conventional camera is aligned with the display center in a dark room, full-screen white stimuli are displayed, and images are captured across vertical incident angles from -10° to

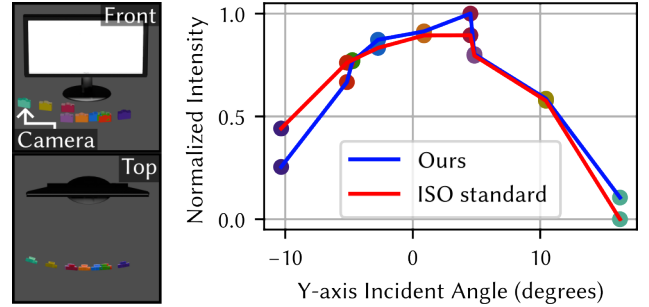


Figure 6: The illustration of the camera poses and the display (left). The average intensity that normalized to $[0, 1]$ from the ISO standard and ours, with data samples color-coded by the corresponding camera poses (right).

16° . The average intensity curves in Fig. 6 show that our method reproduces the similar trend in the ISO setup, validating its physical plausibility. Unlike the ISO standard, our lensless camera setup captures light field data from nine positions on the display without rotating the camera or using controlled lighting. This reduces measurement time and simplifies view-dependent calibration, while maintaining accuracy comparable to the ISO method.

Table 2: Model Comparison

Methods	PSNR (dB) \uparrow	SSIM \uparrow	MSSIM \uparrow
Ours	19.54	0.9165	0.9549
Vanilla	9.93	0.5327	0.8049

Limitations and Future Works. Our 46.6° angular coverage is below the 240° specified in professional display calibration. Future improvements with larger aperture arrays and optimized diffusers could extend this range. Additionally, pixel-wise training limits scalability for full-panel characterization. Several research directions offer potential solutions to these limitations. One is an end-to-end pipeline that removes PSF convolutions, cropping, and padding. Another is the use of emerging Gaussian splatting representations, which model light fields with fewer parameters than INR.

References

- [1] Ziyang Chen, Mustafa Dogan, Josef Spjut, and Kaan Akşit. 2024. SpecTrack: Learned Multi-Rotation Tracking via Speckle Imaging. In *SIGGRAPH Asia 2024 Posters*. 1–2.
- [2] International Organization for Standardization. 2008. ISO 9241-305:2008(E) – Ergonomics of human-system interaction – Part 305: Optical laboratory test methods for electronic visual displays. <https://www.iso.org/standard/39091.html>. Accessed: 2025-06-16.
- [3] Jongyoon Kim, Dae-Heung Lee, Joun-Ho Lee, and Ji-Hoon Lee. 2022. Optimization of the display viewing angle for automotive application. *Journal of Information Display* 23, 1 (2022), 87–95.
- [4] Oliver Kingshott, Nick Antipa, Emrah Bostan, and Kaan Akşit. 2022. Unrolled primal-dual networks for lensless cameras. *Optics Express* 30, 26 (2022), 46324–46335.
- [5] Ben Mildenhall, Pratul P Srinivasan, Matthew Tancik, Jonathan T Barron, Ravi Ramamoorthi, and Ren Ng. 2021. Nerf: Representing scenes as neural radiance fields for view synthesis. *Commun. ACM* 65, 1 (2021), 99–106.